Effects of Boundary Layer Formation on the Vortical Flow above Slender Delta Wings

Dietrich Hummel[#]
Institute of Fluid Mechanics
Technical University Braunschweig
Bienroder Weg 3, D-38106 Braunschweig, Germany

D.Hummel@tu-bs.de

ABSTRACT

The present knowledge about the effects of boundary layer formation on the vortical flow around slender delta wings is summarized. For sharp leading edges the primary flow separation is fixed. On the upper surface laminar flow separation leads to a large secondary vortex, which shifts the primary vortex upwards and inboard, and the corresponding pressure distribution shows a suction peak due to the primary vortex and a suction peak of the same amount due to the secondary vortex. Turbulent flow separation on the upper surface causes only a small secondary vortex, and the reduced shift of the primary vortex leads to a higher suction peak underneath the primary vortex and a lower suction peak underneath the secondary vortex. For CFD code validation a complete set of experimental data for laminar boundary layers on both sides of an A = 1 delta wing is presented. For rounded leading edges the primary flow separation is discussed in detail. Downstream of a region of attached flow in the front part of the wing laminar flow separation takes place, starting on the upper surface and quickly approaching the leading edge. Further downstream transition laminar/turbulent occurs at the leading edge. The primary separation line moves to the upper surface and the primary vortex is considerably weakened. For very high Reynolds numbers turbulent boundary layers near the apex of the wing lead to a delay of the onset of vortices. In order to increase the understanding of vortical flows and to provide new experimental data for validation of CFD codes, a new International Vortex Flow Experiment (VFE-2) is presently under way. Its aims, its organisation and its program of work are briefly summarized and some very first result are presented.

1. INTRODUCTION

On slender wings inclined against the free stream at an angle of attack α, the flow on the lower side moves outboard. Flow separations take place at sharp as well as at rounded leading edges and a primary vortex is formed over the upper surface of the wing as shown in **Fig. 1**. Underneath this vortex an attached flow is established on the upper side with an attachment line located at the centre line or at some spanwise position between the centre line and the leading edge, depending on the angle of attack. The flow near the wing surface is directed outboard and after having passed the suction peak underneath the primary vortex axis the steep adverse pressure gradient towards the leading edge causes another (secondary) flow separation. A secondary vortex is formed in the region close to the leading edge, and under certain circumstances even a tertiary vortex can be observed underneath the secondary vortex. This vortex formation is well known since a long time.

[#] Prof. Dr.-Ing., retired

Paper presented at the RTO AVT Specialists' Meeting on "Enhancement of NATO Military Flight Vehicle Performance by Management of Interacting Boundary Layer Transition and Separation", held in Prague, Czech Republic, 4-7 October 2004, and published in RTO-MP-AVT-111.

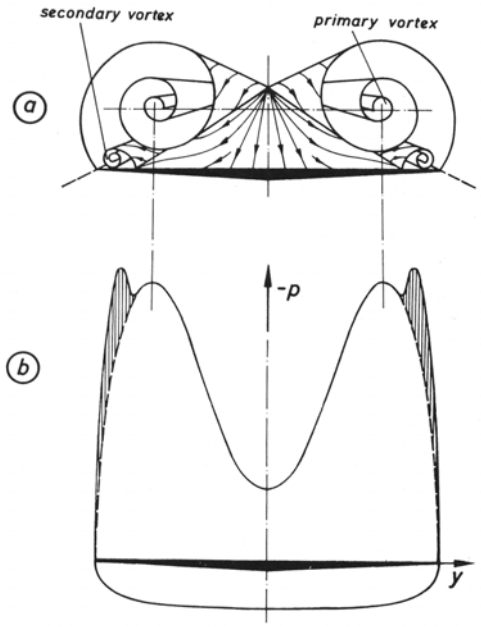

Figure 1: Schematic view of the flow over a sharp edged delta wing.
a) vortex formation b) pressure distribution in a cross section

At the beginning of the 1980's the status of the Euler methods for the calculation of vortical flows had reached such a high standard that good experimental data were necessary to validate the codes. This lead to the International Vortex Flow Experiment (VFE-1) [1], which has been carried out in 1984 – 1986: On a 65° swept cropped delta wing force and pressure distribution measurements as well as flow field studies have been carried out for a certain variety of flow conditions in various wind tunnels worldwide. The results have been summarized in [2], and later the state of the art has been reviewed in [3], [4], [5]. Even for sharp leading edges with fixed primary separation the Euler codes were not well suited to calculate the pressure distribution on a slender wing properly, since the secondary separation was not modelled. In the last ten years considerable progress has been achieved in the numerical calculation of vortical flows by taking into account viscous effects through solutions of the Navier-Stokes equations [6], [7], [8]. Reynolds number effects are now included and secondary vortices turn out. Laminar flow solutions tend to have convergence problems due to weak viscous damping. For turbulent flows in solutions of the Reynolds-averaged Navier-Stokes equations a turbulence model has to be applied, which provides additional viscous damping in the boundary layers as well as in the viscous regions of the vortices. As shown in [9] the pressure distribution on the upper surface of the wing is very sensitive to correct modelling of the viscous regions of the flow field, and this is due to the fact that the status of the boundary layers on the wing has a very strong influence on the formation of the vortices, on their mutual interference and thus on the pressure distribution on the wing.

In the present paper the knowledge on the effects of the boundary layer formation on the vortical flow about slender delta wings is summarized. Since detailed flow field measurements in the viscous regions of a delta wing were beyond the scope of VFE-1, a new and more detailed International Vortex Flow Experiment VFE-2 has been initiated in [9]. This experiment is presently under way as part of the RTO-AVT Panel Task Group AVT-113 entitled "Understanding and Modelling Vortical Flows to Improve the Technology Readiness Level for Military Aircraft". The organization of the VFE-2 facet of this Task Group as well as its program of work will be illustrated, and some preliminary results will be presented.

2. NOTATIONS

b	wing span	δ	boundary layer thickness
c	chord	ξ	dimensionless longitudinal coordinate [= x/c_r]
$\bar{c}$	mean aerodynamic chord	η	dimensionless spanwise coordinate [= $y/s_1(x)$]
c_p	pressure coefficient [= $(p - p_\infty)/q_\infty$]	Λ	leading edge sweep
d	wing maximum thickness		
r	leading edge radius	Indices	
$s_1(x)$	local semispan		
x, y, z	wing fixed coordinates, origin at apex	mac	quantity based on mean aerodynamic chord
A	aspect ratio	r	root chord
M	Mach number	tr	transition
R	Reynolds number [=$V_\infty \cdot c_r/\nu$]	E	outer edge of boundary layer
V	velocity	LE	leading edge
α	angle of attack	W	wing surface
β	streamlines inclination angle (Fig.13)	∞	free stream

3. BOUNDARY LAYER EFFECTS ON WINGS WITH SHARP LEADING EDGES

For wings with sharp leading edges the primary separation is fixed to the leading edges. The flow separates there in any case, and a Reynolds number effect on the primary separation does not exist.

3.1 Effect of the status of the boundary layers

On the surface of the wing boundary layers develop, which depend on the Reynolds number. On both sides of the wing the boundary layer flow starts laminar at the apex of the wing, and under natural conditions far more downstream transition to the turbulent state will take place depending on the Reynolds number. **Fig. 2a,b** shows oil flow patterns on a delta wing A = 1 at $R = 9 \cdot 10^5$ for an angle of attack α = 20.5°. In this case the boundary layers were laminar on both sides of the wing up to the trailing edge [10]. The secondary separation line on the suction side of the wing is clearly indicated. In order to study the general effect of the status of the boundary layer on the vortex formation, the suction side flow has been triggered by means of a turbulence generator located at half semispan as shown in **Fig. 2c**. Thus an artificially turbulent boundary layer has been created, which shifted the secondary separation line towards the leading edge. This effect can be recognized from a comparison of the Figs. 2b and 2c. In the case of a laminar boundary layer the early flow separation leads to a large secondary vortex in the region between the secondary separation line and the leading edge, whereas in the case of a turbulent boundary layer only a small secondary vortex is formed.

The effect of the different secondary vortex formations on the pressure distribution in various cross sections of the wing may be taken from **Fig. 3**. In the laminar case according to Fig.3a the suction peaks underneath the primary vortex are relatively low and they are located far inboard and the suction peaks underneath the secondary vortex are almost as large as those underneath the primary vortex. In the turbulent case the suction peaks underneath the primary vortex are much higher and they are located more outboard than in the laminar case, and the suction peaks underneath the secondary vortex are much lower than those underneath the primary vortex. A direct comparison of the pressure distributions and the

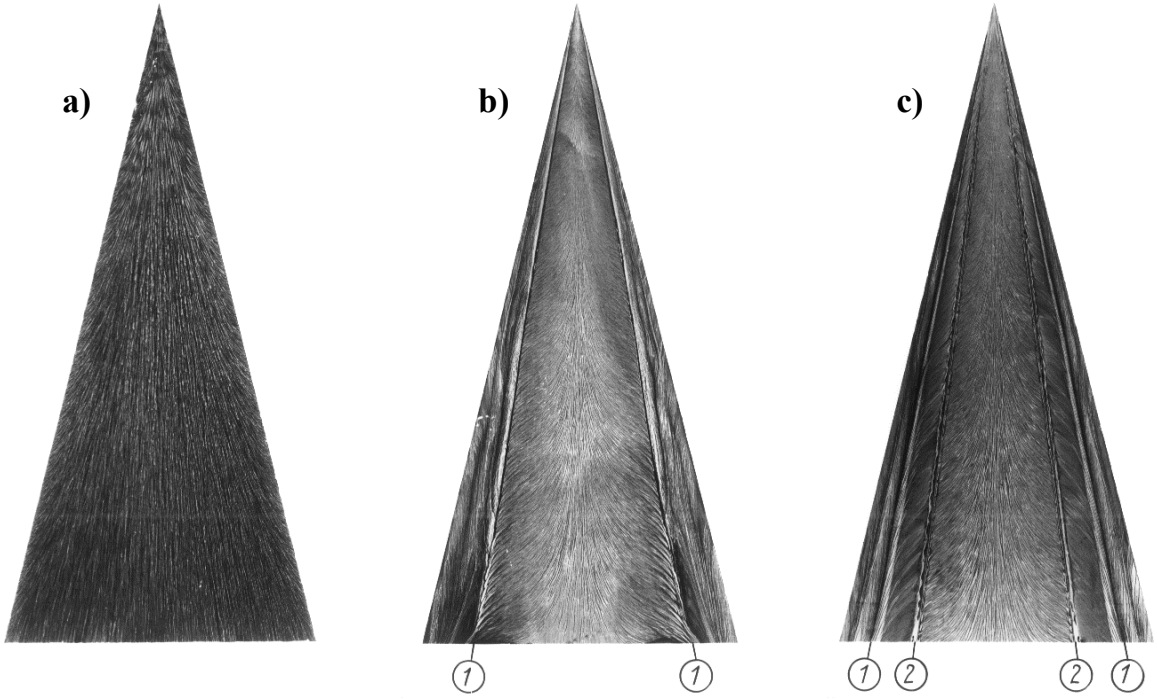

Figure 2 : Oil flow patterns on a delta wing A = 1.0 at R = 9 · 10^5
a) α = 20.5°, pressure side, laminar boundary layer
b) α = 20.5°, suction side, laminar boundary layer
c) α = 20.5°, suction side, artificially turbulent boundary layer
(1) Secondary separation line
(2) Turbulence generator

corresponding secondary vortex formation for both cases at a fixed station at $x/c_r = 0.3$ is shown in **Fig. 4**. The early separation of a laminar boundary layer leads to a large secondary vortex, which shifts the primary vortex upwards and inboard compared with the inviscid case represented in Figs. 3 and 4 by the slender body theory of J.H.B. Smith [14]. Due to the larger distance of the primary vortex from the wing surface the suction peak is considerably lower than that due to inviscid flow and it is located more inboard. Underneath the strong secondary vortex a second suction peak occurs and the suction reaches about the same amount as due to the primary vortex. Below the secondary vortex the flow near the surface of the wing is directed inboard and due to the high suction peak underneath the secondary vortex it passes another adverse pressure gradient which might lead to a tertiary flow separation in the vicinity of the secondary separation line. Such a tertiary vortex formation is indicated in the pressure distribution through a third relative suction peak located between those of the primary and the secondary vortex [11]. In the case of the separation of a turbulent boundary layer the smaller secondary vortex leads to a lower shift of the primary vortex upwards and inboard. Correspondingly the suction peak underneath the primary vortex is larger and due to the smaller additional suction induced by the secondary vortex a pressure distribution with a single suction peak turns out. The inboard flow below the secondary vortex does not experience an adverse pressure gradient and therefore no tertiary separations take place in the case of turbulent flow separations.

The present results indicate that due to the mutual interference between the primary and the secondary vortex characteristic pressure distributions occur on the wing surface, which are significantly different for laminar and turbulent secondary separation. Therefore the measured pressure distributions can be used to tell laminar and turbulent flow separation in experiments without any further investigations on the status of the boundary layers. Due to the strong dependence of the pressure distribution on the status of the

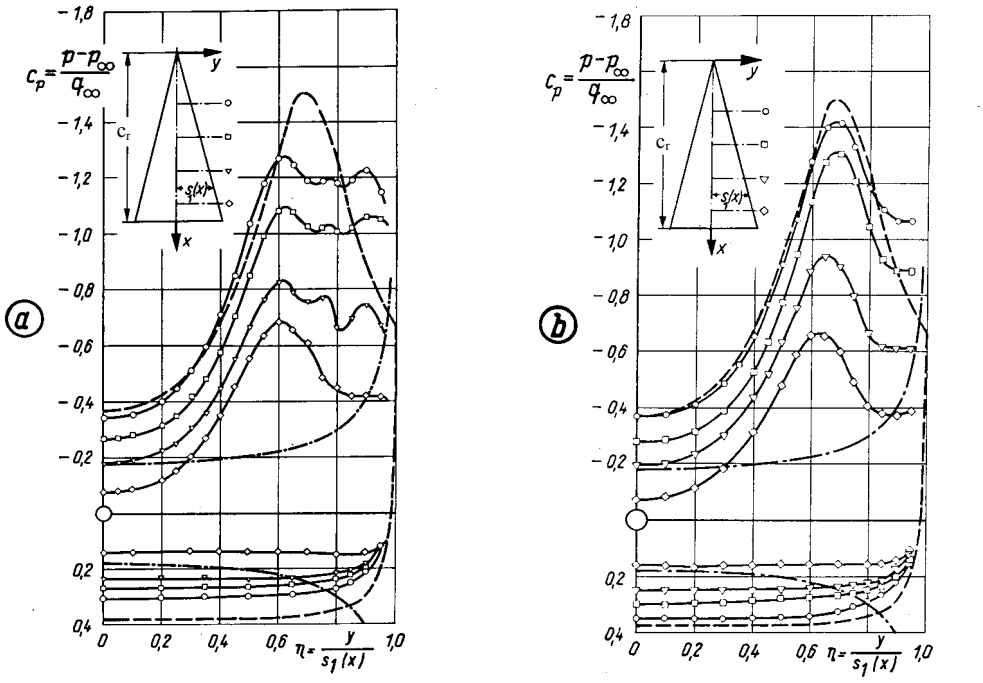

Figure 3: Pressure distributions on delta wing A = 1.0 at α = 20.5°
a) R = 9 · 10^5, laminar boundary layer
b) Artificially turbulent boundary layer
– – – Theory J.H.B. Smith [14]

Figure 4: Pressure distribution and vortex formation on the delta wing A = 1 at α = 20.5° in the section x/c_r = 0.3

a) Pressure distribution

Boundary layer

• laminar

o turbulent

– – – Theory J.H.B. Smith [14]

b) Vortex formation

(schematic)

Boundary layer

—— laminar

– – – turbulent

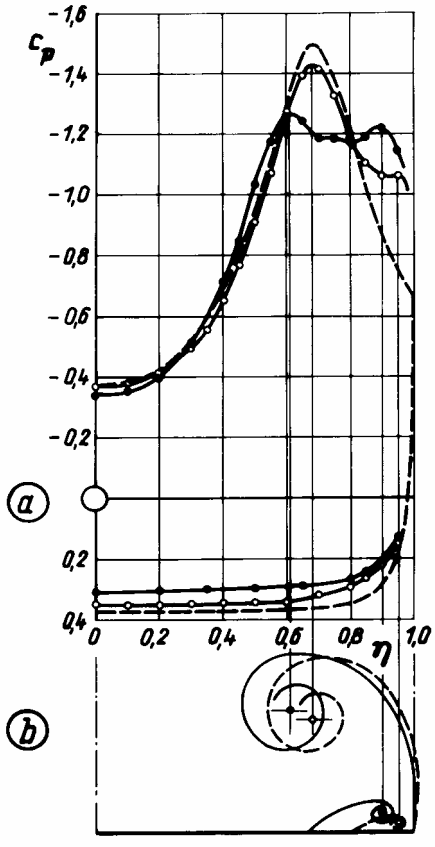

boundary layers reasonable results from numerical calculations of the flow field can only be expected if the boundary layers are covered properly by the numerical code. The position of the secondary separation line and the strength and the structure of the secondary vortex must be calculated precisely in order to achieve reasonable pressure distributions. Another interesting result, which can be drawn from the Figs. 3 and 4, is the fact that the area underneath the pressure distributions is virtually the same for both cases. This means that the overall forces and moments do not significantly depend on the status of the boundary layers although the details of the pressure distributions are very sensitive.

3.2 Effects of Reynolds number

In the preceding section the two cases with fully laminar flow and artificially fully turbulent flow have been considered in order to show the principal differences. In real flow, however, transition from laminar to turbulent boundary layer flow will take place at some location on the wing surface depending on the free stream Reynolds number and on the angle of attack. **Fig. 5** shows oil flow patterns on the suction side of a delta wing A = 1 at $\alpha = 26.4°$ for various Reynolds numbers, which have been adjusted by variation of the free stream velocity. For $R = 0.88 \cdot 10^6$ the flow is laminar almost up to the trailing edge of the wing and the secondary separation line is a straight line up to the trailing edge region. With increasing Reynolds number the flow becomes turbulent in the rear part of the wing. The secondary separation line is straight up to a certain location x_{tr} and from that position onwards it moves towards the leading edge. The turbulent boundary layer is able to endure a steeper adverse pressure gradient and the flow separation is therefore delayed. The amount of x_{tr} reduces with increasing Reynolds number, and at $R = 2.00 \cdot 10^6$ the laminar flow region is confined to a small area in the vicinity of the apex of the wing. For other angles of attack a similar movement of the transition laminar/turbulent takes place, but the distances x_{tr} are different. However, for all Reynolds numbers $R = V_\infty c_r/\nu$ the quantity $R_{tr} = V_\infty x_{tr}/\nu$ has the same value, which depends only on the angle of attack α. The movement of the transition laminar/turbulent with the angle of attack can therefore be described by the function $R_{tr}(\alpha)$, which is shown in **Fig. 6** for the delta wing A = 1. For a given Reynolds number R and a certain value of α the position of transition is determined as $x_{tr}/c_r = R_{tr}(\alpha)/R$.

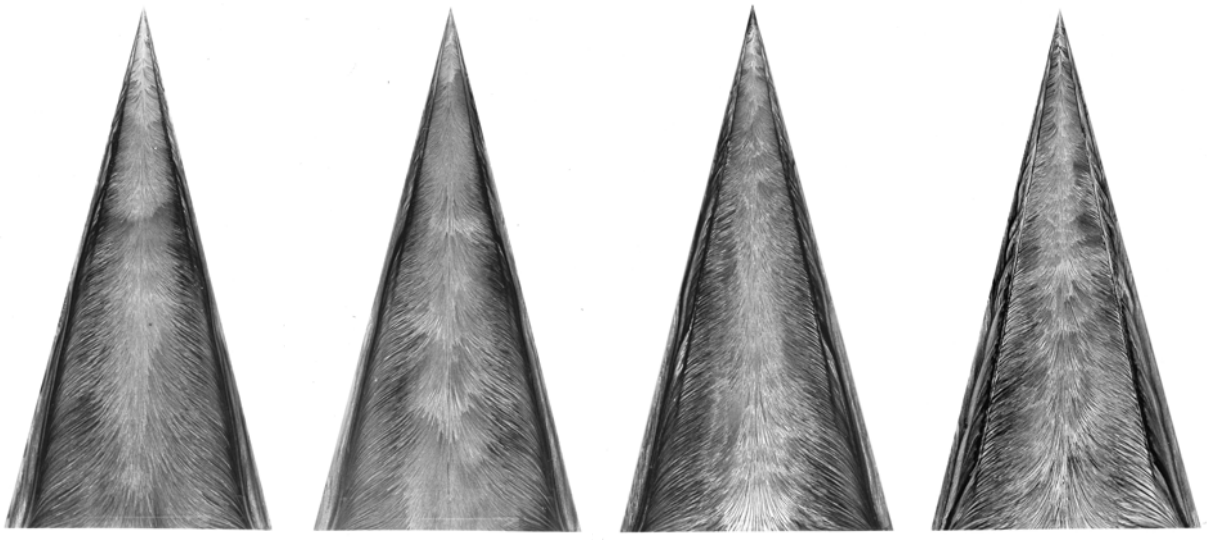

$R = 2.00 \cdot 10^6$ **$R = 1.55 \cdot 10^6$** **$R = 1.27 \cdot 10^6$** **$R = 0.88 \cdot 10^6$**

Figure 5: Effect of Reynolds number on the oil flow patterns on the suction side of a delta wing A = 1 at $\alpha = 26.4°$

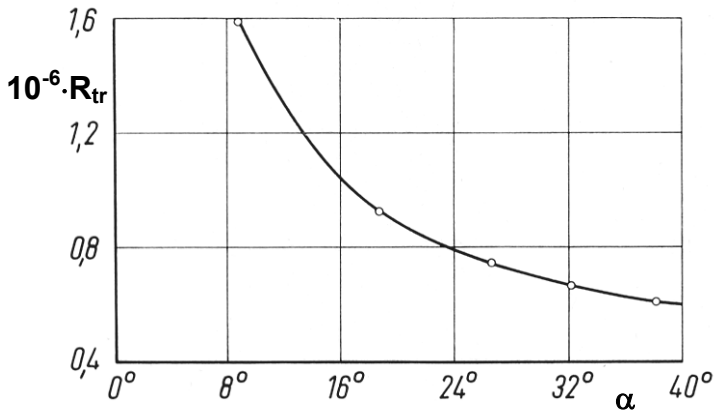

Figure 6: Upstream movement of transition laminar/turbulent with angle of attack on a delta wing A = 1

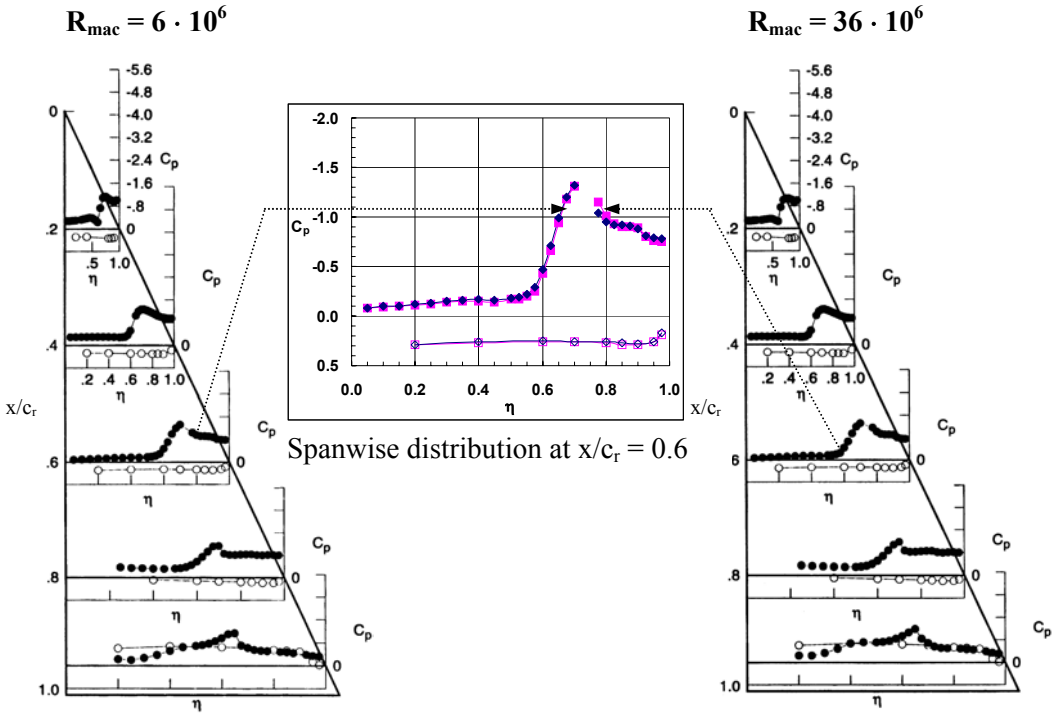

Figure 7: Effect of Reynolds number on the pressure distribution of an A = 1.85 (Λ = 65°) sharp edged delta wing at M = 0.85, α = 13° [16]

For Reynolds numbers $R > 2 \cdot 10^6$ laminar flow separation is confined to a small area near the apex of the wing and turbulent flow separation takes place over the main portion of the wing. Further increasing Reynolds numbers have been covered in the comprehensive pressure distribution measurements carried out at NASA Langley Research Center for an A = 1.85 (Λ = 65°) delta wing [16]. Results for the sharp leading edge as shown in **Fig. 7** indicate that in the region of mainly turbulent secondary separation virtually no Reynolds number effect take place. For a sharp edged wing the status of the lower surface boundary layer has no effect on the vortex formation and the upper surface boundary layer, since the primary separation is fixed to the sharp leading edge in any case.

3.3 Experimental data for comparison with CFD results

For Reynolds numbers R > 10^6 the kink in the secondary separation line is located at x_{tr}. Up to this position laminar flow separates at the laminar secondary separation line. Downstream of this point the boundary layer has passed somewhere the transition point and turbulent separation takes place at the turbulent secondary separation line. On the wing surface there exists a transition line, which connects all transition points and which starts at the kink in the separation line. It is important to note that this transition line is not known. Up to now no systematic investigations have been carried out to determine the regions of laminar and of turbulent flow on a sharp edged delta wing. If a method would come up to predict these regions, we would not be able to validate it due to lack of experimental data. On the other hand CFD calculations can be carried out either for fully laminar or for fully turbulent flow. For very high Reynolds numbers the laminar flow part near the apex of the wing is very small, and calculations for fully turbulent flow are justified in this case. For moderate Reynolds numbers, however, in CFD calculations for turbulent boundary layers the laminar front part should be taken into account properly and this could be done using an experimentally determined transition location, but unfortunately experiments of this kind are missing up to now. It is one of the aims of the new VFE-2 to close this gap and to perform this kind of measurements.
The experimental results of VFE-1 have been mainly compared with inviscid flow calculations. The pressure distribution on the wing surface was not well predicted by the solutions of the Euler equations, since the secondary separation was not modelled at all. Today viscosity is taken into account by solving the Navier-Stokes equations and a secondary vortex turns out. For comparison with numerical results experimental 3D boundary layer data are available only in a single paper [13]: For the A = 1 delta wing according to Fig. 2a,b at $\alpha = 20.5°$ and $R = 9 \cdot 10^5$ the upper and lower surface boundary layers have been measured using a flat 3-hole probe. In this case the boundary layers were laminar everywhere on the wing. These experimental data are not well known, and since they might be used for comparison with CFD results some details may be described subsequently.

The wing geometry is shown in **Fig. 8**. The A = 1 delta wing has a flat upper surface and a flat triangular cross section. The largest relative thickness is $d/c_r = 0.021$ located at $\xi = x/c_r = 0.9$. Underneath the surface of the wing straight pressure tubes are embedded along lines $\eta = y/s_1(x) = \text{const.}$, and pressure

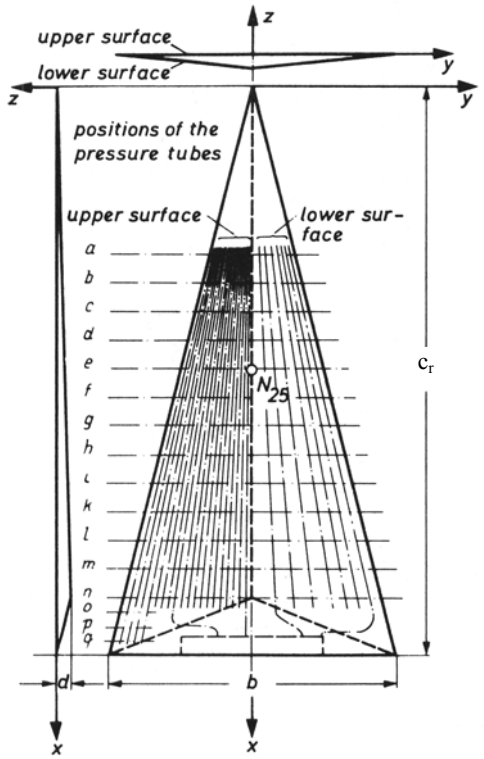

Figure 8: Geometry of the delta wing A = 1

N_{25} Quarter chord point of mean aerodynamic chord, located at $x/c_r = 0.5$.

Dimensions:
Wing root chord $c_r = 750$ mm
Wing span b = 375 mm
Maximum wing thickness d = 16 mm

tabs are located in sections $0.3 \leq \xi \leq 0.9$ (steps $\Delta\xi = 0.05$), see a … q. Results of six component balance measurements on this wing may be taken from [11] and [13], and pressure distributions are given in [13]. The boundary layer measurements have been carried out on the flat surface of the wing. This means that the lower surface boundary layer has been measured for $\alpha = -20{,}5°$ and that on the upper surface for $\alpha = 20.5°$.

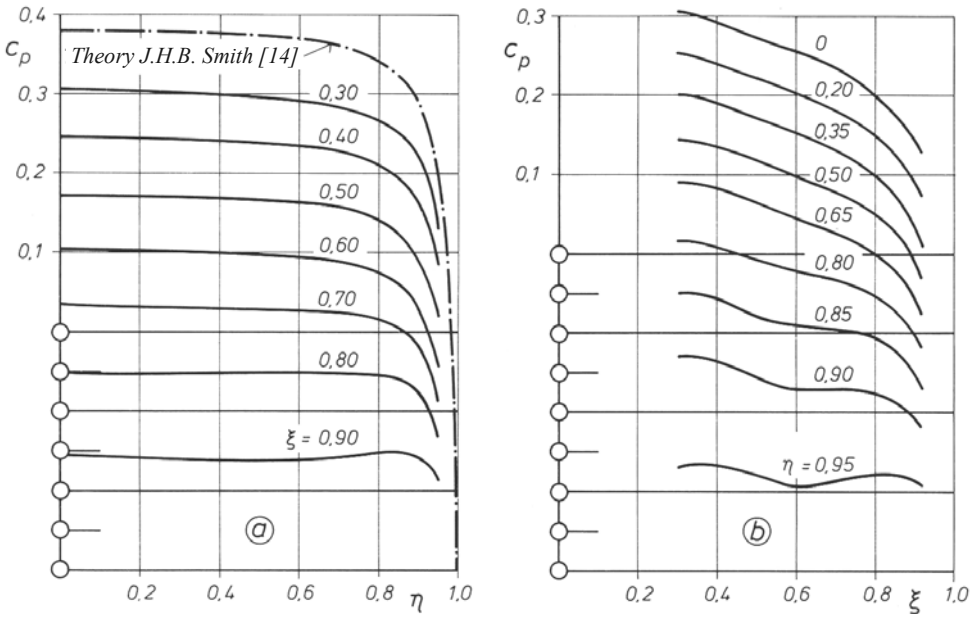

Figure 9: Pressure distribution on the delta wing A = 1
at α = -20.5° (flat side, lower surface)) at R = 9 · 10^5
a) in cross sections ξ = const.
b) along rays η = const.

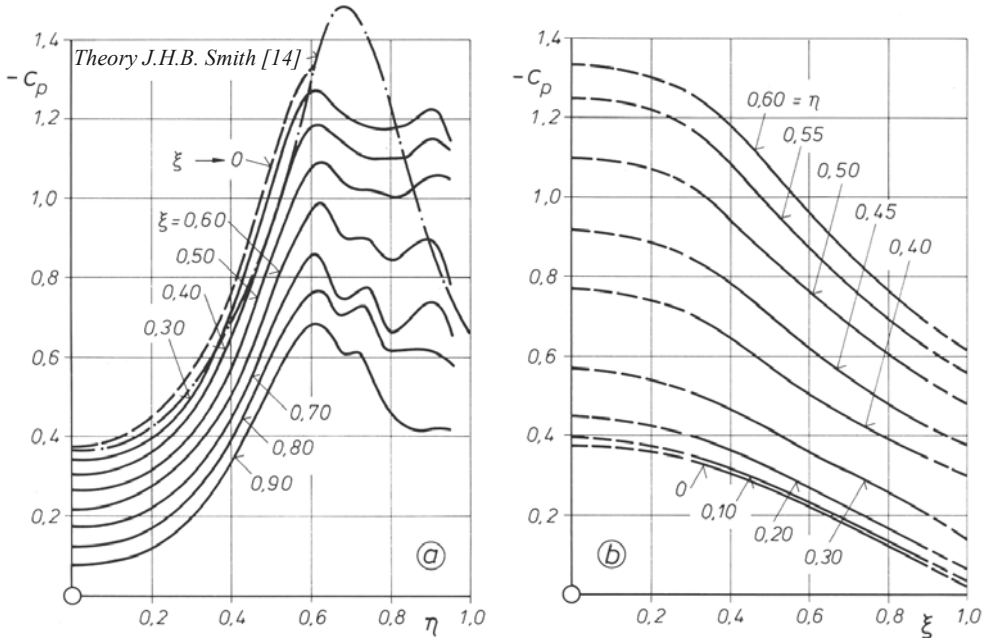

Figure 10: Pressure distribution on the delta wing A = 1
at α = 20.5° (flat side, upper surface)) at R = 9 · 10^5
a) in cross sections ξ = const.
b) along rays η = const.

The measured pressure distributions are shown in **Figs. 9 and 10** for the lower and the upper surface respectively. Numerical values for these distributions may be taken also from tables in [13]. The shape of the upper surface pressure distribution clearly indicates the separation of a laminar boundary layer as well as the formation of a tertiary vortex underneath the secondary vortex [11]. For Euler and Navier-Stokes calculations these pressure distributions turn out, but for calculations according boundary layer theory these pressure distributions have to be prescribed.

Concerning some details of the boundary layer measurements the boundary layer thickness is shown in **Figs. 11 and 12** for the lower and the upper side of the wing. The boundary layer thickness on the pressure side is larger than that on the suction side, and on both sides the boundary layer thickness increases towards the trailing edge of the wing. On both sides the velocity profiles are twisted. In **Fig. 13** the inclinations $ß_E$ of the velocity vectors at the outer edge of the boundary layer are plotted as functions of $\xi = x/c_r$ and $\eta = y/s_1(x)$. The corresponding values for the limit at the wing surface $ß_W$ have been determined from the surface oilflow patterns according to Fig. 2a,b and they are included in Fig. 13. The difference between $ß_E$ and $ß_W$ represents the twist of the velocity profiles. On the suction side the secondary separation lines are located at $\eta = \pm 0.68$. Numerical values for the measured inclinations are available in [13]. On the pressure side the twist of the velocity profiles increases with increasing distance from the centre line of the wing and it decreases towards the trailing edge. The largest twist occurs in the region of accelerated flow towards the leading edge where according to Fig. 11 the boundary layer is very thin. On the suction side the velocity profiles are even more twisted, and again the largest twist occurs in the region of the accelerated flow underneath the primary vortex where the boundary layer is thin. On both sides of the wing the inclination of the velocity vector depends mainly on the spanwise coordinate η, whereas the values are almost constant along rays η = const. This means that the flow is almost conical with respect to the flow direction. Over a large portion of the wing the suction peak due to the primary vortex is located at $\eta = \pm 0.62$.

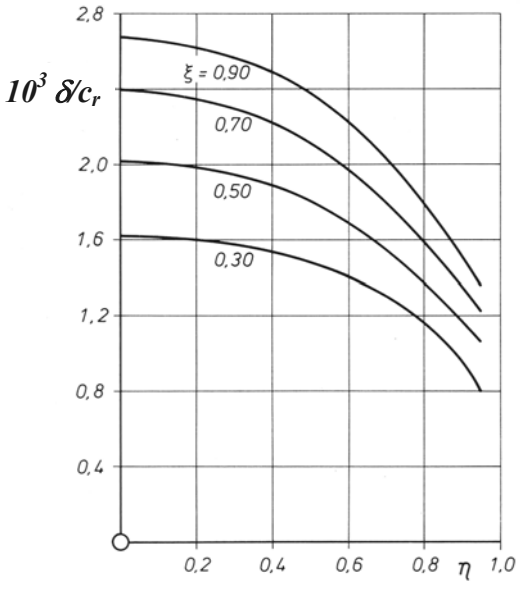

Figure 11: Boundary layer thickness on the pressure side of the delta wing A = 1 at α = -20.5°, R = 9 · 10^5

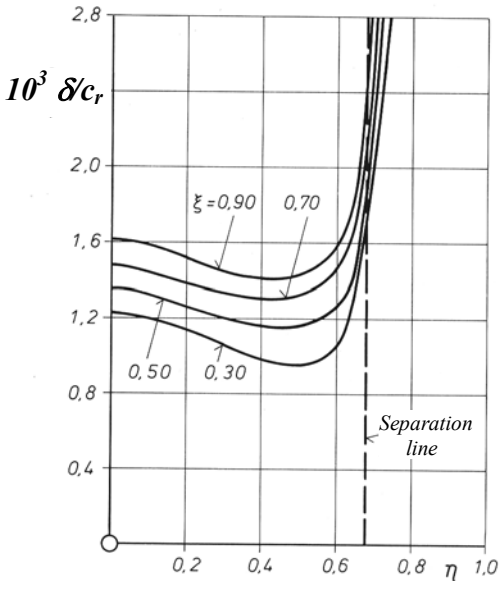

Figure 12: Boundary layer thickness on the suction side of the delta wing A = 1 at α = 20.5°, R = 9 · 10^5

The boundary layer measurements under consideration [13] have been used for comparison with an early attempt to calculate the laminar boundary layer for given pressure distribution using boundary layer theory. Two different methods have been developed in [15]: In the “small cross flow” method the full

momentum integral equation is applied in the direction of the outer flow, whereas in cross flow direction only a considerably simplified momentum integral equation has been used. In the "quasi conical" method a finite difference solution of the boundary layer equations is calculated for an inviscid outer flow with constant inclination angle $ß_E$ and variable velocity V_E along rays η = const. In the calculations variations of the flow quantities along rays η = const. are considered to be small compared to variations in directions normal to rays η = const. These assumptions describe the measured situation very well. The flow is actually not conical, but it can be considered as locally conical. For details of both methods see [15]. A typical comparison of calculated and measured velocity profiles is presented in **Fig. 14** for the

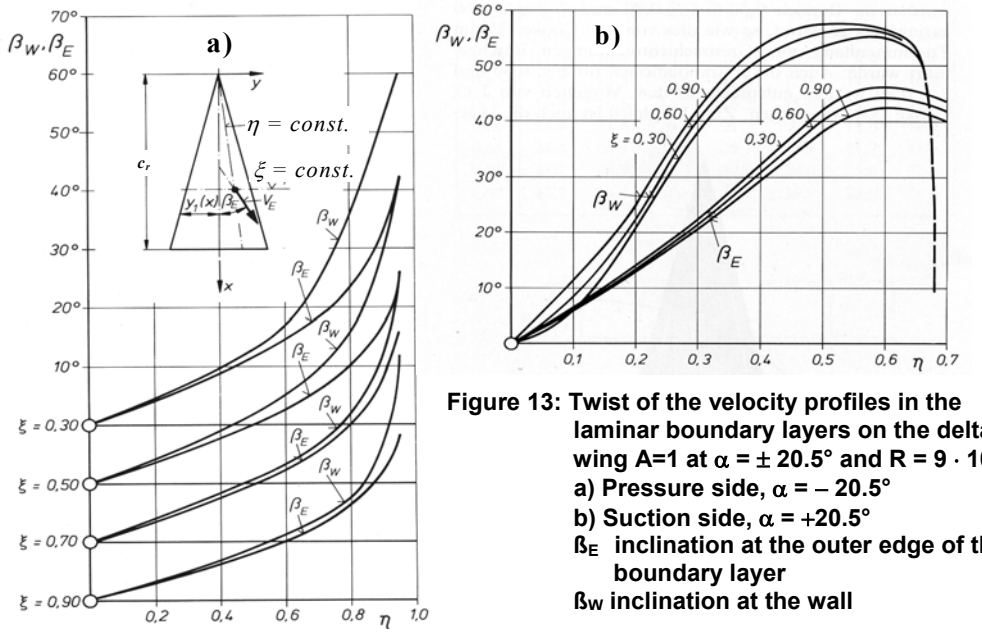

Figure 13: Twist of the velocity profiles in the laminar boundary layers on the delta wing A=1 at $\alpha = \pm 20.5°$ and $R = 9 \cdot 10^5$
a) Pressure side, $\alpha = -20.5°$
b) Suction side, $\alpha = +20.5°$
$ß_E$ inclination at the outer edge of the boundary layer
$ß_W$ inclination at the wall

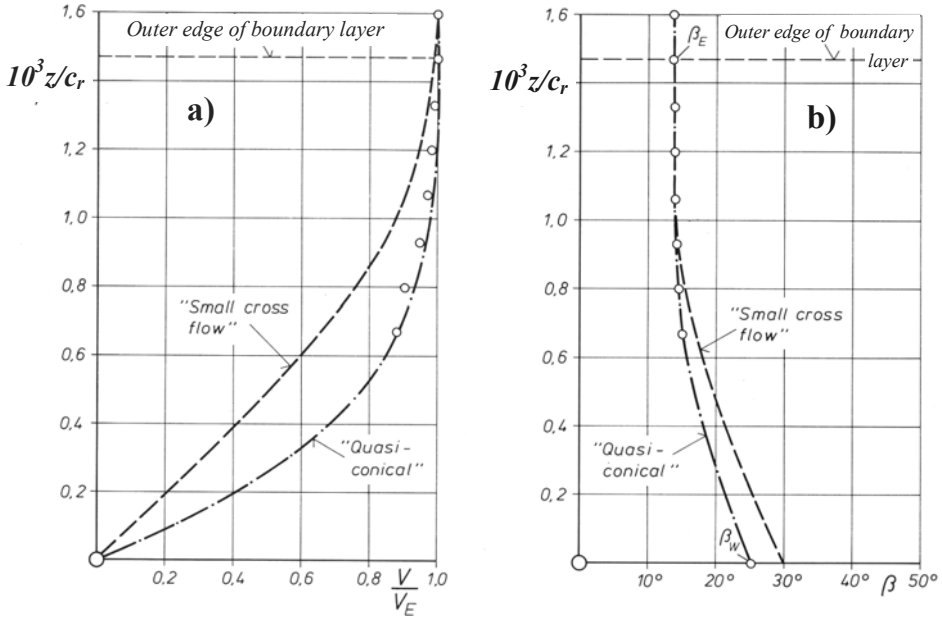

Figure 14: Velocity profile in the laminar boundary layer on the suction side of the delta wing A = 1 at the location $\xi = 0.90$, $\eta = 0.20$ for $\alpha = 20.5°$ and $R = 9 \cdot 10^5$. Comparison of measurements [13] with theoretical results according to J.C. Cooke [15]
a) Velocity distribution V/V_E b) Distribution of local inclination ß

location $\xi = 0.90$ and $\eta = 0.20$. The distributions of the amount of the velocity and of the twist are plotted against the distance from the wing surface. The "quasi conical" approach shows excellent agreement with the experimental data, whereas the results according to the "small cross flow" method are not correct. In the present situation the "quasi conical" flow assumptions are justified. It is interesting to note that in these measurements experimental data were available for the outer portion of the boundary layer only, since the probe technique did not allow to get closer to the wing surface. Nevertheless these data were sufficient to check the validity of the two methods.

4. BOUNDARY LAYER EFFECTS ON WINGS WITH ROUNDED LEADING EDGES

For wings with rounded leading edges the primary flow separation is no longer enforced by the leading edge shape. In the front part of the wing even an attached flow region may exist. Further downstream primary flow separation takes place somewhere in the leading edge region, but the separation line is no longer fixed to the leading edge. Its position depends on the status of the separating boundary layer being either laminar or turbulent. This means that the boundary layer status at the leading edge effects the formation of the primary vortex on the upper surface of the wing. Underneath the primary vortices the upper surface boundary layer formation virtually takes place according to the principles described for the sharp leading edge case in section 3.

4.1 Primary separation

4.1.1 Attached flow

At the apex of the wing the flow starts laminar on both sides of the wing. For the wing with rounded leading edge at low angles of attack a region of attached flow is established on the upper surface of the wing as shown in **Fig. 15**, taken from [16]. The attached flow is indicated by the high suction at the leading edge.

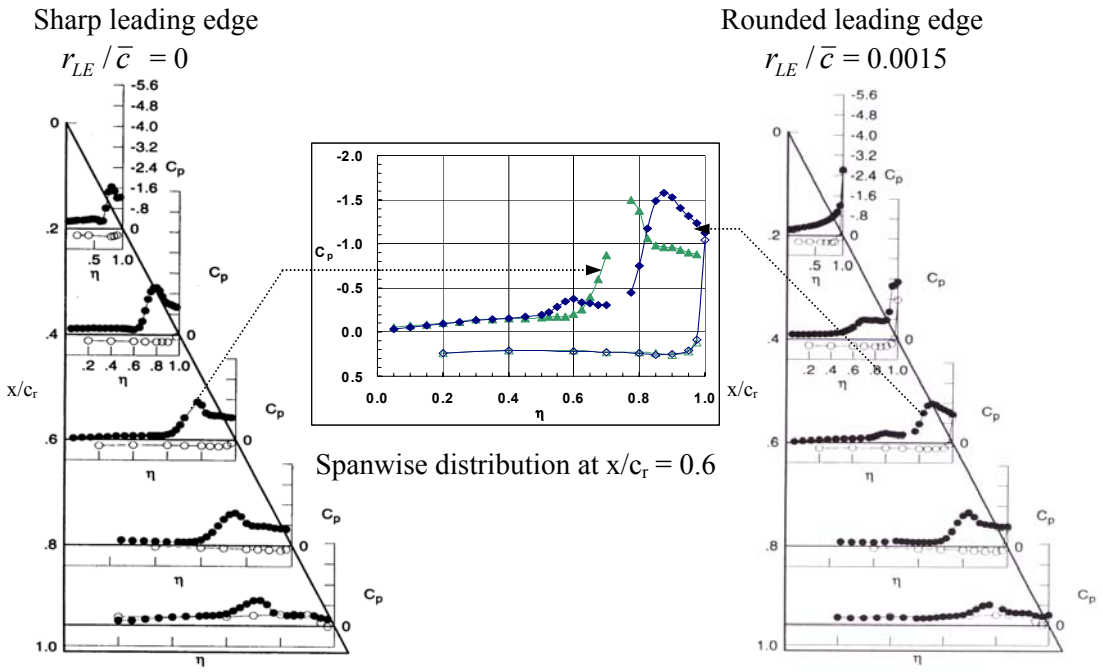

Figure 15: Effect of leading edge bluntness on the pressure distribution of an A = 1.85 (Λ = 65°) delta wing at M = 0.4, $R_{mac} = 6 \cdot 10^6$, α = 13°, [16]

4.1.2 Laminar separation

Further downstream (see Fig.15, rounded leading edge, x/c_r = 0.4) the laminar flow around the leading edge still causes high suction at the leading edge, but the steep adverse pressure gradient leads to a primary separation, which starts on the upper surface, and the pressure distribution indicates the presence of a primary vortex above the wing surface. More downstream two effects are observed: 1) The primary separation line quickly approaches the leading edge and then the high suction at the leading edge disappears for sections $x/c_r \geq 0.6$. Although the status of the boundary layers has not been documented in [16] it can be assumed that the lower surface boundary layer is laminar and that in the rear part of the rounded leading edge wing according to Fig.15 laminar separation at the leading edge forms the primary vortex on the upper side of the wing. 2) The first primary vortex to be formed is located far inboard at η = 0.7 (see Fig.15, rounded leading edge, section at x/c_r = 0.4) causing a single suction peak, but further downstream pressure distributions with two suction peaks are observed (see section x/c_r = 0.6). Finally the inner suction peak disappears or merges into the outer one (see section x/c_r = 0.8). This phenomenon is not understood up to now, and it will be subject to investigations within the new VFE-2 tests.

4.1.3 Turbulent separation

With increasing Reynolds number the boundary layer, which separates at the leading edge, should become turbulent. The lower surface pressure distribution is flat and the flow is accelerated towards the leading edge. Although investigations on the status of the lower surface boundary layer are missing it can be assumed that up to high Reynolds numbers the lower surface boundary layer remains laminar up to the leading edge. At the leading edge, however, instead of laminar separation transition to the turbulent state of the boundary layer must be expected. This has been found in [17] for an A = 1.1 delta configuration with elliptic cross sections over a large portion of the rear part of the body. **Fig. 16** shows the geometry

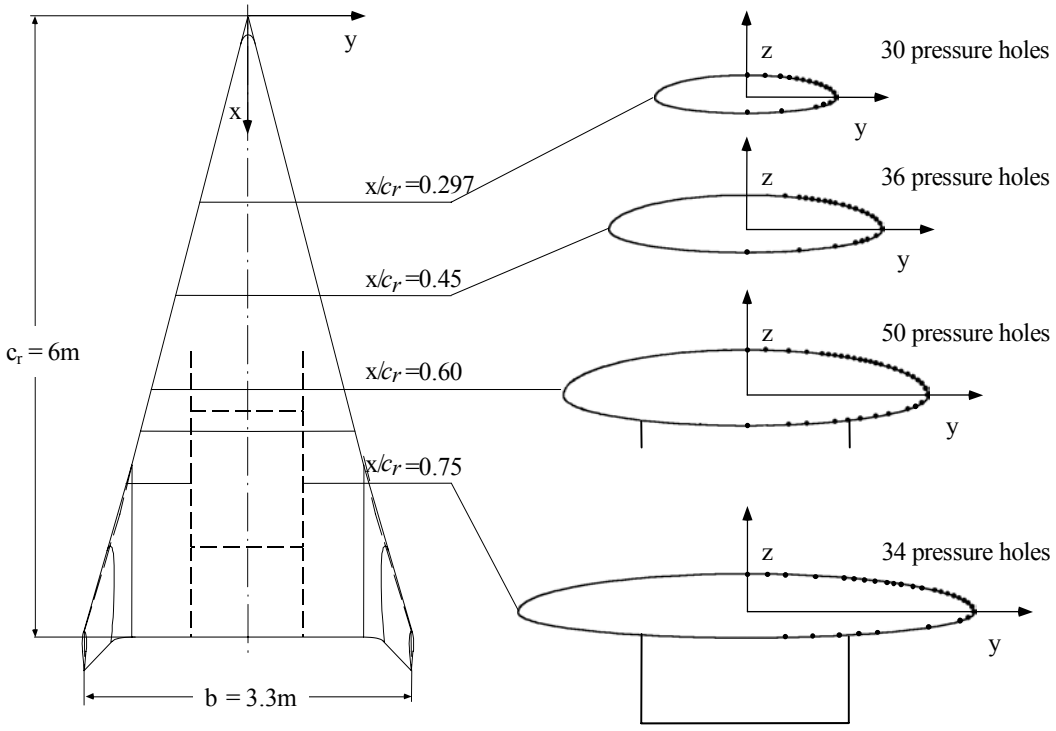

Figure 16: ELAC-1 configuration with elliptic cross sections, A = 1.1 (Λ = 75°), [17]

according to [17] and in **Fig. 17** the pressure distribution in the cross section at $x/c_r = 0.3$ is plotted for $\alpha = 12°$ and for various Reynolds numbers. For $R = 7.9 \cdot 10^6$ and $R = 11.9 \cdot 10^6$ in the cross section at $x/c_r = 0.3$ laminar flow separation takes place at the leading edge and a strong primary vortex is formed over the upper surface of the wing. With increasing Reynolds number transition laminar/turbulent takes place at the leading edge. For $R \geq 19.8 \cdot 10^6$ the transition onset point on the leading edge has passed already the section at $x/c_r = 0.3$ under consideration as shown in **Fig. 18**. Starting at $x/c_r = 0.15$ the primary separation line is shifted to the upper surface of the wing, since the turbulent boundary layer is able to sustain the adverse pressure gradient to a certain amount without separation. Suddenly high suction peaks are observed at the leading edge caused by the attached flow around the leading edge. Due to the delay of the primary separation the corresponding primary vortex is weakened and it is located far inboard at $\eta = 0.64$. This process starts in the rear part of the configuration and proceeds upstream with increasing Reynolds number [17].

A very comprehensive data set for a 65° delta wing with one sharp and three rounded leading edges is available in [16]. Pressure distribution measurements have been carried out for a large variety of Mach numbers and Reynolds numbers. This data set contains the effect of Reynolds number on the pressure distribution for cases with part span vortex formation, i.e. attached flow in the front part and separated flow in the rear part, for extremely different Reynolds numbers. **Fig. 19** show results for the medium radius leading edge configuration at $M = 0.4$ and $\alpha = 13°$ at $R_{mac} = 6 \cdot 10^6$ (see Fig.15) and at $R_{mac} = 72.7 \cdot 10^6$. For the lower Reynolds number the onset of a primary vortex is due to laminar flow separation as discussed in sections 4.1.1 and 4.1.2, and the region of attached flow near the apex of the wing extends to about $x/c_r = 0.3$. For the very high Reynolds number, however, the flow in the region of attached flow is turbulent. Therefore the vortex formation due to turbulent flow separation is delayed and the region of attached flow extends up to $x/c_r = 0.6$.

The behaviour of the flow around the leading edge is governed by the parameters Reynolds number and leading edge radius. A schematic view of the flow along a rounded leading edge is shown in **Fig. 20**. Moving downstream, in the leading edge region the following flow phenomena may be observed: 1) Laminar flow around the leading edge without flow separation. 2) Laminar flow around the leading edge

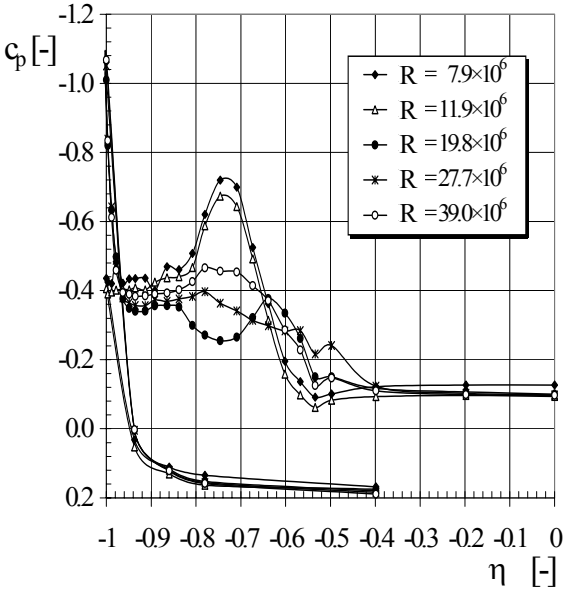

Figure 17: Effect of Reynolds number on the pressure distribution of the ELAC-1 configuration in the section $x/c_r = 0.3$ at $\alpha = 12°$ [17]

Figure 18: Oil flow patterns on the front part of the ELAC-1 configuration at $\alpha = 12°$ for $R = 19.8 \cdot 10^6$ [17]
(1) primary separation line
(2) secondary separation line

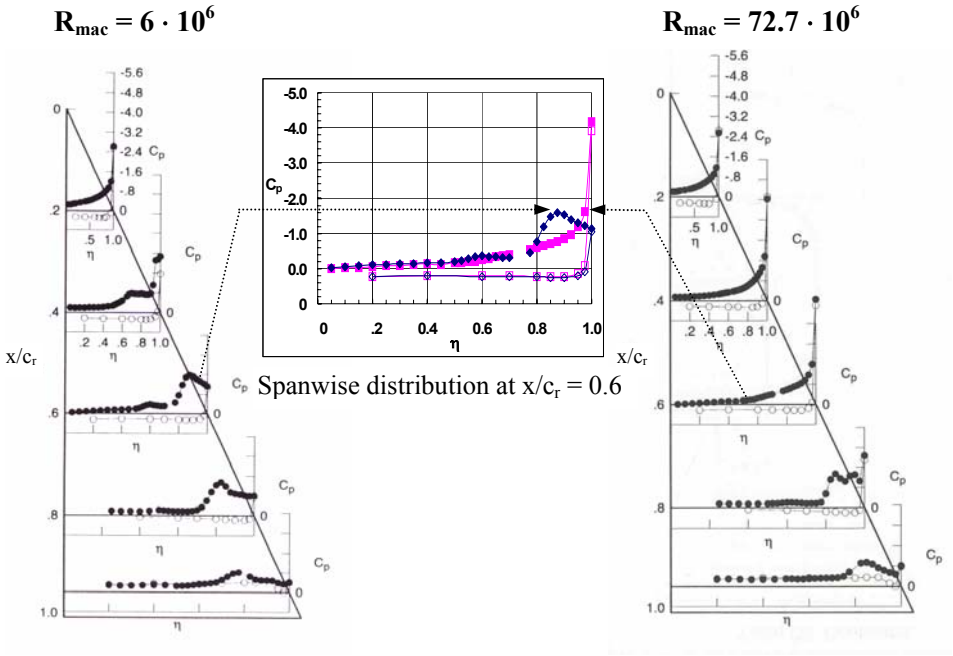

Figure 19: Effect of Reynolds number on the pressure distribution of an A = 1.85 (Λ = 65°) delta wing with rounded leading edge (r_{LE} / $\bar{c}$ = 0.0015) at M = 0.4, α = 13°, [16]

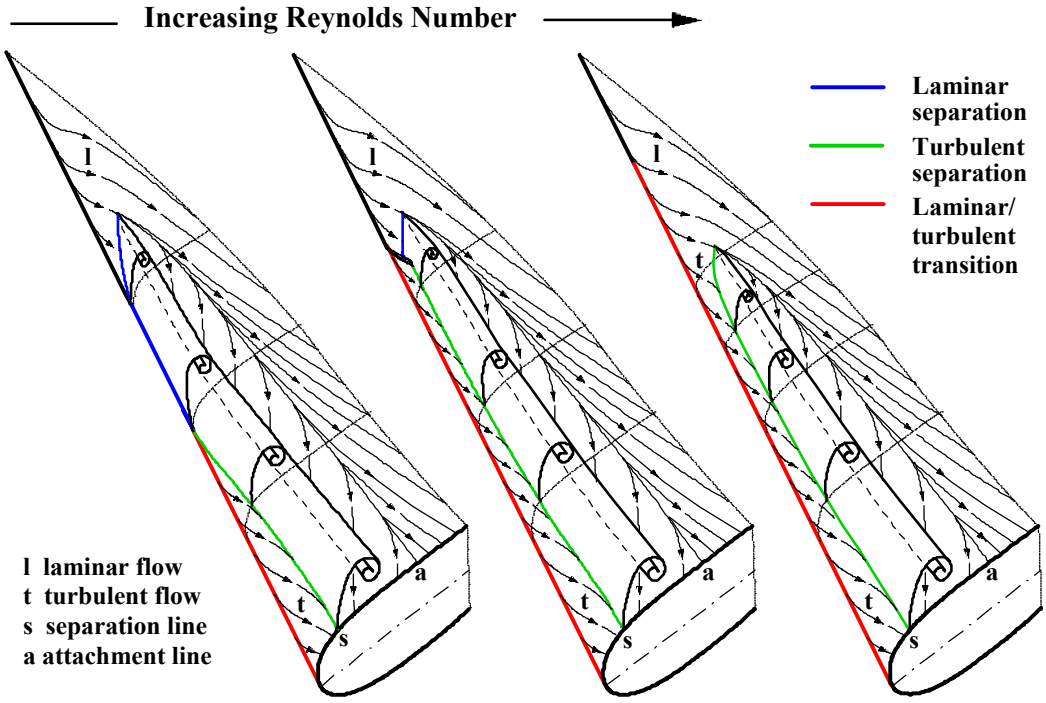

Figure 20: Effect of Reynolds number on the primary vortex formation along a rounded leading edge (schematic, secondary separations left out)

followed by the onset of laminar flow separation on the upper surface of the wing. 3) The laminar separation line on the upper surface moves towards the leading edge and laminar flow separation occurs at the leading edge. Moving further downstream the local Reynolds number increases: 4) Laminar flow separation ends at a certain point along the leading edge and is then replaced by laminar/turbulent transition. The primary separation line is shifted again to the upper surface. Along the displaced primary separation line turbulent separation takes place. With increasing Reynolds number the point of transition laminar/turbulent at the leading edge moves upstream and the region of laminar primary separation is reduced more and more, and finally the laminar primary separation disappears at all and along the whole primary separation line turbulent flow separation takes place. However if the transition laminar/turbulent reaches the apex region of the wing the onset of a primary vortex resulting from turbulent flow separation is delayed as compared with the laminar case, since the turbulent boundary layer is better suited to withstand the adverse pressure gradients. Therefore the region of attached flow in the apex region is larger for the turbulent case at high Reynolds numbers than for the laminar case at low Reynolds numbers. With decreasing leading edge radius the displacements of the primary separation line at the onset of laminar separation and in the whole region of turbulent separation are reduced, and for very small leading edge radii the primary separation occurs at the leading edge as in the case of a sharp leading edge.

4.2 Secondary separation

Underneath the primary vortex the flow attaches as in the case of a sharp edged wing. The vortex sheet emanating from the separation line merges into the vortex center whereas the attachment line is formed by other streamlines originating from the free stream. Therefore regions of laminar and turbulent boundary layer flow develop on the upper surface in the same way as for sharp edged wings and the same effects on the displacement of the primary vortex and corresponding modifications of the pressure distribution due to the secondary vortex formation are expected. These effects have been discussed in detail in section 3, and they will not be repeated here.

5. VORTEX FLOW EXPERIMENT 2

5.1 New measurements

In modern CFD solutions of the RANS equations various turbulence models are used. In such calculations the 3D turbulent boundary layer in the attached flow regime on the upper surface of the wing, the position of the secondary separation line and the structure of the secondary vortex should be covered properly in order to predict the pressure distribution accurately. Results for different turbulence models show a considerable amount of scatter. For a detailed comparison with measurements the well known results of the first vortex flow experiment VFE-1 [1], [2] are no longer sufficient, and therefore a new vortex flow experiment VFE-2 has been proposed in [9].

For VFE-2 a $\Lambda = 65°$ delta wing was chosen, corresponding to an aspect ratio of $A = 1.85$. This geometry leads to a favourable partitioning of the angle of attack range into certain flow regimes:

i) Attached flow without vortex formation $0° \le \alpha \le 4°$
ii) Separated vortical flow without vortex breakdown $4° \le \alpha \le 20°$
iii) Separated vortical flow with vortex breakdown $20° \le \alpha \le 40°$
iv) Separated deadwater-type flow $40° \le \alpha \le 90°$.

Boundary layer measurements could be carried out quite easily for flat upper and lower surfaces of the wing. Interchangeable sharp and rounded leading edges should be available, and the rear sting for positioning in the wind tunnel should be as small as possible. All these requirements are fulfilled by the NASA configuration [16], shown in **Fig 21**. The wing consists of an inner flat plate part and interchangeable leading edges with four different radii. The whole geometry including the sting is described by means of analytical formulas.

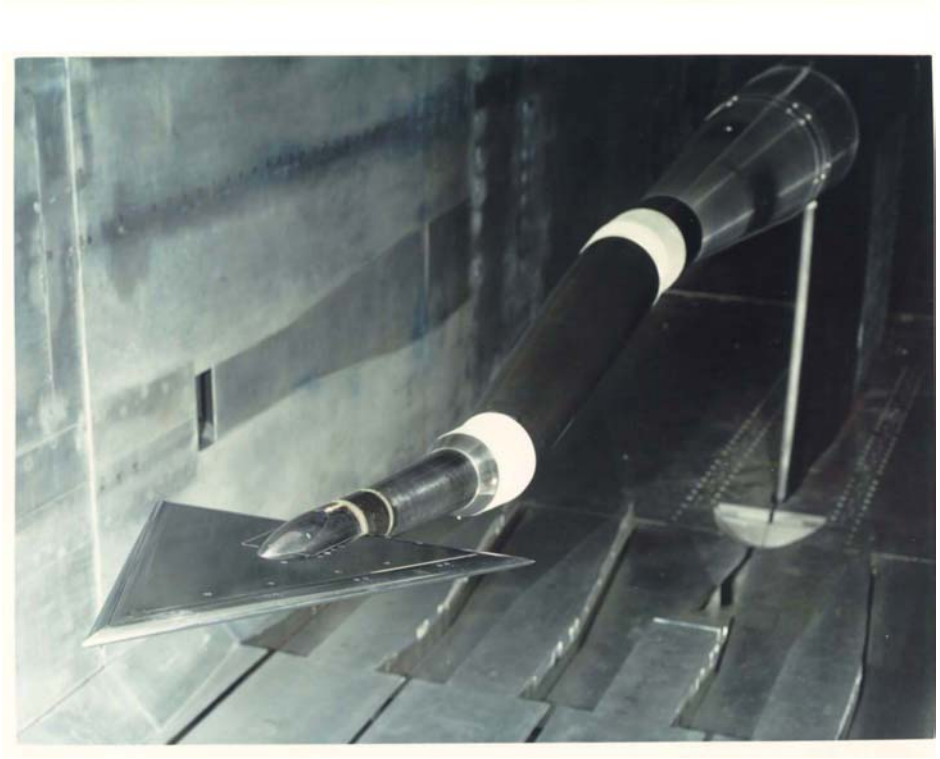

Figure 21: Λ = 65° (A = 1.85) delta wing at cryogenic tests in the National Transonic Facility (NTF), NASA Langley Research Centre, [16] (by courtesy of J.M. Luckring)

For the Λ = 65° delta wing comprehensive measurements of lift, pitching moment, and of the pressure distribution in sections at x/c_r = 0.2; 0.4; 0.6; 0.8 and 0.95 have been carried out at NASA for a large variety of Mach numbers and Reynolds numbers. The predominant part of these investigations has been performed on a large model in the National Transonic Facility (NTF) at NASA Langley RC, and the results are published in [16]. In addition some unpublished results of measurements at low Mach numbers and low Reynolds numbers on a smaller wind tunnel model in the Low Turbulence Pressure Tunnel (LTPT) at NASA Langley RC are available. These two sets of measurements are the starting point for VFE-2. In an international cooperation additional measurement will be carried out for the NASA configuration. They will be mainly concentrated on the flow field around the delta wing comprising

- Detection of transition laminar/turbulent
- Detailed pressure distribution measurements, especially in the region of the onset of flow separation for rounded leading edge configurations
- Boundary layer measurements including distributions of the components of velocity and vorticity, of turbulent energy and eddy viscosity
- Determination of the wall shear stress and detection of the secondary and tertiary separation lines
- Flow field measurements in the primary and secondary vortices including components of velocity and vorticity, turbulent energy and eddy viscosity.

Concerning the Mach number and Reynolds number ranges, only some of the new investigations will be closely related to the NTF matrix investigated by NASA [16], whereas most of the new measurements will

be carried out for incompressible flows, represented by the LTPT results of NASA. Another huge matrix for possible investigations is given by the available four leading edge shapes and by the large variety of angles of attack, which lead to various flow regimes. The new measurements will mainly concentrate on rounded leading edges, and sharp leading edges will be used for reference only. Three angles of attack, corresponding to three different flow regimes, will be studied in detail. These are

- Onset of vortical flow, $\alpha = 13°$
  - Sharp leading edge: Separated flow
  - Rounded leading edge: Partly attached, partly separated flow
- Separated flow without vortex breakdown, $\alpha = 18°$
  - Sharp leading edge
  - Rounded leading edge
- Separated flow with vortex breakdown, $\alpha = 23°$
  - Sharp leading edge
  - Rounded leading edge

For the sharp edged delta wing configuration the vortical flow becomes unsteady over the wing for $\alpha = 23°$, and the well-known spiral form of vortex breakdown occurs in the primary vortices. In this case, in addition to the study of the bluntness effects on this phenomenon, special investigations will be aimed at the frequency of the surface pressure fluctuations on the wing in the vortex breakdown region.

The experimental investigations within VFE-2 will be used to validate the available CFD codes. For this purpose a common structured and a common unstructured grid for the relatively simple delta wing configuration including the sting will be used by the participants in order to check the capability of their codes and to improve them.

5.2 Organization

The new International Vortex Flow Experiment VFE-2 is presently carried out within the framework of an RTO Task Group of the Applied Vehicle Technology (AVT) panel

Task Group AVT-113: Understanding and Modelling Vortical Flows to Improve the Technology Readiness Level for Military Aircraft.

Co-chairmen are Dr. John E. Lamar, NASA Langley RC, US, and Prof. Dr. Dietrich Hummel, TU Braunschweig, Germany. The Task Group consists of two facets

- **F-16XL facet (Cranked Arrow Wing Aerodynamics Project International, CAWAPI)**
  This group performs numerical calculations for the complete aircraft F-16XL and compares the results with already existing flight test data for various angles of attack and Mach numbers at full scale Reynolds numbers
- **65° Delta Wing facet (International Vortex Flow Experiment 2, VFE-2)**
  This group performs new wind tunnel experiments in order to understand the vortical flow and uses their experimental results to validate existing CFD codes

Between both facets a close cooperation takes place, since almost all participants of the F-16XL facet validate their CFD codes also for the VFE-2 configuration. For communication among each other, within each facet a Virtual Laboratory (VL) is used, which allows to upload and download surface geometries, grids, experimental data, numerical results, etc.

The AVT-113 Task Group has been prepared after the AVT Symposium on “Vortex Flow and High Angle of Attack”, held in Loen, Norway, 7 – 11 May 2001, see [9], and it came into operation in spring 2003.

5.3 Program of Work

After one year of activity the program of work (POW) for AVT-113 has been fixed in spring 2004. The key issues for the VFE-2 facet may be summarized as follows:

- The NASA results for the NTF and the LTPT investigations will be made available through the Virtual Laboratory. NASA Langley RC has placed their smaller LTPT wind tunnel model at disposal for tests in other wind tunnels worldwide. A loan agreement has been signed for the transfer of the model to Germany (DLR, Goettingen), and further loan agreements with France (ONERA, Lille), Turkey (TUBITAK-SAGE, Ankara) and Sweden (FOI, Stockholm) are in progress, (Dr. J. Luckring).
- The NASA wind tunnel model is presently at its first stage in Goettingen. A new sting for use in European wind tunnels has been produced. The model will be tested in the Transonic Wind Tunnel Goettingen (TWG) in July/August 2004 (PSP measurements) and in February 2005 (PIV measurements), (Dr. R. Konrath).
- A new (second) wind tunnel model is being built at TU Munich (Germany). It will be used to perform hot-wire measurements in the boundary layers and in the vortical flow field in the low speed wind tunnels of Institute for Fluid Mechanics, TU Munich. The first wind tunnel entry is planned for autumn 2004, (Dr. Ch. Breitsamter).
- A third wind tunnel model is presently manufactured at University of Glasgow (UK). The model is aimed at new steady and unsteady balance and pressure distribution measurements as well as for PIV investigations. First tunnel entry will take place in early 2005, (Prof. F. Coton).
- The American wind tunnel model will move to ONERA, Lille (France) in 2005. New balance measurements as well as PIV investigations will be carried out, (Dr. O. Rodriguez).
- The American wind tunnel model will move to TUBITAK-SAGE (Turkey) in 2005/06. The measurements will concentrate on the laminar/turbulent transition, (Mr. S. Kurun).
- Finally the wind tunnel model will move to the Swedish Defence Research Institute FOI (Sweden). Details are presently under consideration, (Dr. P.-A. Torlund).
- For the VFE-2 numerical calculations the common unstructured grids for the sharp and the medium radius leading edge will be provided by NASA Langley RC (Dr. S. Pirzadeh) with contributions by USAFA Colorado (Prof. S. Morton) and KTH Stockholm (Prof. A. Rizzi). The corresponding structured grids will be provided by ONERA, Lille (Dr. O. Rodriguez, Dr. F. Le Roy). These will be available in spring 2005.

5.4 First results

The first wind tunnel entry of the NASA wind tunnel model in the Transonic Wind Tunnel Goettingen (TWG) took place from 22 July to 16 August 2004. The configurations with the medium radius leading edges as well as with the sharp leading edges were tested in the angle of attack range $0° \le \alpha \le 25°$. First of all pressure distribution measurements have been carried out using the surface pressure tabs of the model in combination with PSI modules. In the NTF tests at NASA the lowest Reynolds number was $R_{mac} = 6 \cdot 10^6$ for all Mach numbers, and this value could be achieved in the TWG Goettingen for M = 0.8 and 0.85 only. For these conditions a direct comparison of the results was possible and an excellent agreement turned out. This fact is remarkable, since in the two tests different wind tunnel models have been investigated in different wind tunnels, in which different ratios of the model size relative to the tunnel dimensions were present. The PSI pressure distribution measurements were mainly carried out for Mach numbers M = 0.3/0.4/0.6/0.8 and 0.85 and for Reynolds numbers $R_{mac} = 3 \cdot 10^6$ and $2 \cdot 10^6$. A comparison of results would be possible for the LTPT tests at NASA Langley RC, but these data are not yet available. The measurements for M = 0.3, $R_{mac} = 2 \cdot 10^6$ form the link to the future measurements in incompressible flow, for which a maximum Reynolds number of $R_{mac} = 2 \cdot 10^6$ is expected.

During the first wind tunnel entry in the TWG Goettingen pressure distribution measurements by means of the Pressure Sensitive Paint (PSP) technique have been carried out by the DLR-PSP team for M = 0.4 and 0.8 and $R_{mac} = 3 \cdot 10^6$ and $2 \cdot 10^6$ in the angle of attack range $10° \leq \alpha \leq 25°$. As a first result of these tests the upper surface pressure distribution is shown in **Fig. 22** for the configuration with the medium radius leading edge at M = 0.4, $R_{mac} = 3 \cdot 10^6$ and $\alpha = 13°$. In the region of the beginning vortex formation the NTF results according to Fig. 15 had shown spanwise pressure distributions with two suction peaks of different size. The same is found in the present PSI results (Fig. 22a) as well as in the coloured PSP picture (Fig. 22b) and in the detailed PSP results for various sections (Fig. 22c). The flow separation starts at $x/c_r = 0.34$ on the upper surface and at $x/c_r = 0.4$ a weak vortex can be detected in the region $0.50 \leq \eta \leq .$ 0.85. The strong vortex starts close to the leading edge at $x/c_r = 0.5$ and develops further downstream, but the inner weak vortex is still present and can be identified in all downstream sections.

On the basis of these findings the schematic view of the vortex formation along a rounded leading edge according to Fig. 20 has to be detailed concerning the onset of laminar flow separation as shown in **Fig. 23**: In the front part the laminar flow separates on the upper surface and forms a relatively weak vortex, which contains only a small portion of vorticity and which produces additional suction in the region underneath. More downstream the separation line moves towards the leading edge and in this region high vorticity is shed into the separated flow regime. A strong (double-branched) vortex is formed and more downstream a tendency towards mixing of the weak inner vortex into the strong outer vortex exists. However the formation of the first laminar flow separation is very sensitive to disturbances, and therefore the vortex formation is slightly unsymmetrical as indicated in Fig. 22b and correspondingly the mixing process of the two vortices is different on both sides. On the right-hand side the two vortices remain separate, whereas on the left-hand side the two vortices merge definitely.

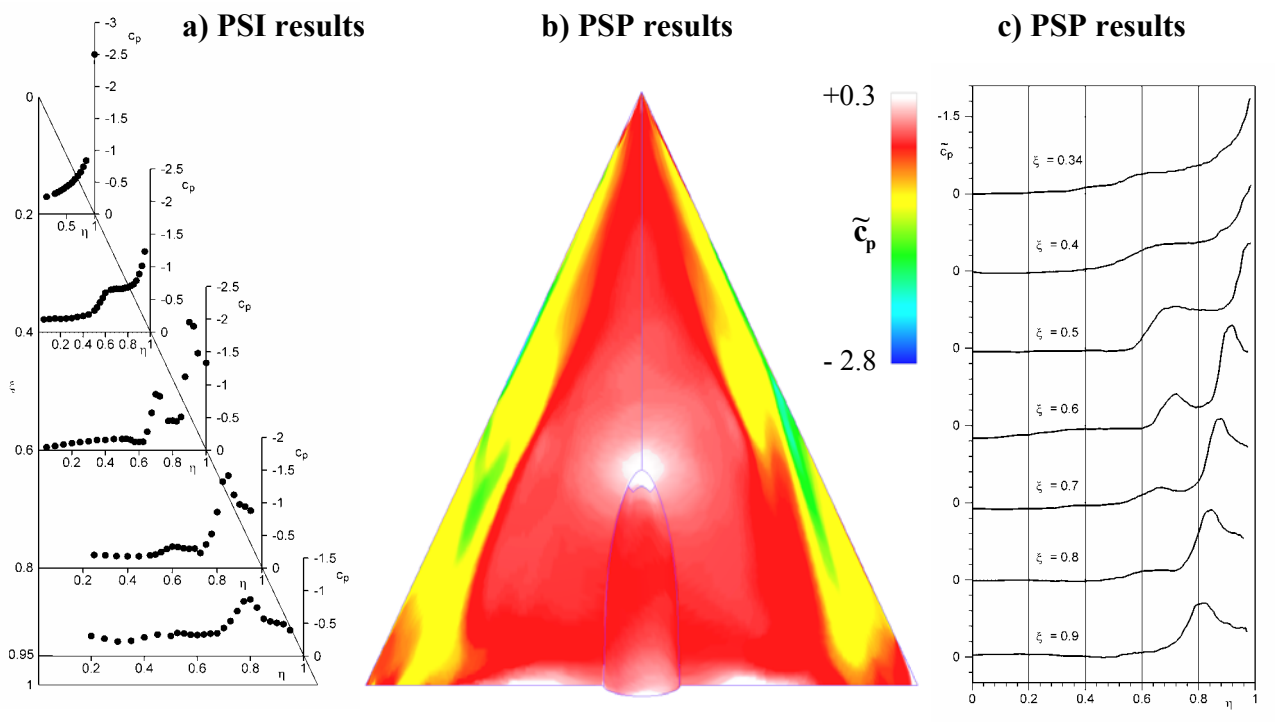

Figure 22: Pressure distribution on the delta wing A = 1.85 (Λ = 65°) with rounded leading edges ($r/\overline{c} = 0.0015$) for M = 0.4, $R_{mac} = 3 \cdot 10^6$, $\alpha = 13°$. First results from DLR Göttingen, $\tilde{c}_p$ preliminary pressure coefficients without PSP offset correction

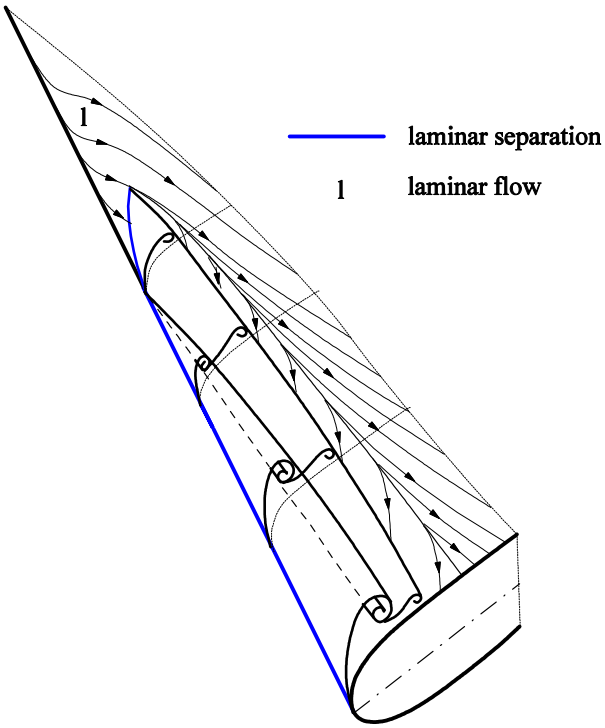

In further studies within VFE-2 the first laminar flow separation should be studied in more detail and its relation to a laminar separation bubble should be clarified. Surface oilflow patterns and investigations on laminar/turbulent transition will be carried out in other wind tunnels for incompressible flow, and the various PIV investigations should be used to check the validity of the flow field structure proposed in Fig. 23.

Fig. 23: Onset of the vortical flow at a rounded leading edge through laminar separation on the upper surface and along the leading edge (schematic, secondary separations left out). Formation of a twin vortex system

6. CONCLUSIONS

In this paper the effects of the boundary layer status on the vortex formation and the pressure distribution on delta wings has been analyzed in detail. For wings with **sharp leading edges** laminar boundary layers lead to a more inboard location of the primary vortex and to a strong secondary vortex with high suction underneath, whereas turbulent boundary layers cause a more outboard located primary vortex and a weaker secondary vortex with only small additional suction. For laminar flow 3D boundary layer measurements on an A = 1 delta wing are presented. For wings with **rounded leading edges** the present knowledge on the primary vortex formation is summarized. Near the apex of the wing a region of attached flow is present. Further downstream laminar flow separation takes place on the upper surface of the wing and still further downstream along the leading edge. In the rear part of the wing transition laminar/ turbulent takes place and turbulent separation occurs again on the upper surface of the wing. A schematic view of the effect of Reynolds number on the primary vortex formation is given, see Fig. 20.

The new **Vortex Flow Experiment 2** (VFE-2), which is presently being carried out within the framework of the RTO AVT Task Group 113, is briefly described and the scientific program of work is outlined. The tests in various wind tunnels have just started, and in this paper first and preliminary results of PSP tests in the Transonic Wind Tunnel Goettingen (TWG) are presented: The primary vortex formation on a wing with rounded leading edge is governed by a twin vortex system originating from a weak and inboard located laminar separation on the upper surface and followed by a strong separation originating from the leading edge and located close to the leading edge. This first understanding of the flow topology at the border between attached and separated flow has to be checked by further tests in the course of VFE-2.

7. REFERENCES

[1] Drougge, G.: The international vortex flow experiment for computer code validation. ICAS-Proceedings 1988, Vol. 1, pp. XXXV-XLI.

[2] Elsenaar, A.; Hjelmberg, L; Bütefisch, K.-A. and Bannink, W.J.: The international vortex flow experiment. AGARD-CP 437 (1988), Vol. 1, pp. 9-1 to 9-23.

[3] Wager, B.; Hitzel, S.; Schmatz, M.A.; Schwarz, W.; Hilgenstock, A. and Scherr, S.: Status of CFD validation on the vortex flow experiment. AGARD-CP 437 (1988), Vol. 1, pp. 10-1 to 10-10.

[4] Hoeijmakers, H.W.M.: Modelling and numerical simulation of vortex flow in aerodynamics. AGARD-CP 494 (1991), pp. 1-1 to 1-46.

[5] Luckring, J.M.: Recent progress in computational vortex-flow aerodynamics. AGARD-CP 494 (1991), pp. 6-1 to 6-21.

[6] Hilgenstock, A. and Vollmers, H.: On the simulation of compressible turbulent flows past delta wing, delta wing-body and delta wing-canard. AGARD-CP 494 (1991), pp. 7-1 to 7-13.

[7] Williams, B.R.; Kordulla, W.; Borsi, M. and Hoeijmakers, H.W.M.: Comparison of various Euler solvers and one Navier-Stokes solver for the flow about a sharp-edged cropped delta wing. AGARD-CP 494 (1991), pp. 2-1 to 2-12.

[8] Borsi, M.; Kordulla, W.; Hoeijmakers, H.W.M. and Williams, B.R.: Comparisons of solutions of various Navier Stokes solvers and one Euler solver for the flow about a sharp-edged cropped delta wing. In: Royal Aeron. Soc. (Ed.): Proceedings of the 1993 European Forum on "Recent Developments and Applications in Aeronautical CFD", Bristol 1993, pp. 5.1 – 5.11.

[9] Hummel, D. and Redeker, G.: A new vortex flow experiment for computer code validation. RTO AVT Symposium on "Vortex Flow and High Angle of Attack Aerodynamics", Loen, Norway, 7 – 11 May 2001,Meeting Proceedings RTO-MP-069 (I), SYA-8/1 to 8/31 (2003).

[10] Hummel, D.: Experimentelle Untersuchung der Strömung auf der Saugseite eines schlanken Deltaflügels. Z. Flugwiss. 13 (1965), 247 – 252.

[11] Hummel, D.: Zur Umströmung scharfkantiger schlanker Deltaflügel bei großen Anstellwinkeln. Z. Flugwiss. 15 (1967), 376 – 385.

[12] Hummel, D. and Redeker, G.: Experimentelle Bestimmung der gebundenen Wirbellinien sowie des Strömungsverlaufs in der Umgebung der Hinterkante eines schlanken Deltaflügels. Abhandlg. d. Braunschw. Wiss. Ges. 22 (1972), 273 – 290.

[13] Hummel, D.: Experimentelle Untersuchung dreidimensionaler laminarer Grenzschichten an einem schlanken Deltaflügel. Zeitschr. f. Flugwiss. u. Weltraumforschg. 10 (1986), 133 –145.

[14] Smith, J.H.B.: Improved calculations of leading-edge separation from slender delta wings. RAE TR 66070 (1966).

[15] Cooke, J.C.: Laminar boundary layer calculations compared with measurements by Hummel. RAE TR 67227 (1967), ARC CP 1096 (1967).

[16] Chu, J. and Luckring, J.M.: Experimental surface pressure data obtained on 65° delta wing across Reynolds number and Mach number ranges. NASA TM 4645 (1996).

[17] Neuwerth, G., Peiter, U. Decker, F. and Jacob, C.: Reynolds number effects on the low speed aerodynamics of the hypersonic configuration ELAC-1. AIAA Paper 98-1578 (1998).